REPORT DOCUMENTATION PAGE

Form Approved
OMB No. 0704-0188

1. REPORT DATE *(DD-MM-YYYY)*	2. REPORT TYPE	3. DATES COVERED *(From - To)*
September 4, 2003	Performance Report	05/15/03 - 08/31/03

4. TITLE AND SUBTITLE
Modification, Assembly and Characterization of Biological

Evolved Electronic and Magnetic Hybrid Materials

5a. CONTRACT NUMBER

5b. GRANT NUMBER
F49620-03-1-0319

5c. PROGRAM ELEMENT NUMBER

6. AUTHOR(S)
Angela M. Belcher

5d. PROJECT NUMBER

5e. TASK NUMBER

5f. WORK UNIT NUMBER

7. PERFORMING ORGANIZATION NAME(S) AND ADDRESS(ES)

Massachusetts Institute of
Technology
77 Massachusetts Avenue
Cambridge, MA 02139

8. PERFORMING ORGANIZATION REPORT NUMBER

9. SPONSORING / MONITORING AGENCY NAME(S) AND ADDRESS(ES)
Air Force Office of Scientific Research
DoD - Miscellaneous; Defense Technical Information Center
Attention: DTIC-OCP
8725 John J. Kingman Road, Suite 0944
Fort Belvoir, VA 22060-6218

10. SPONSOR/MONITOR'S ACRONYM(S)
AFOSR

11. SPONSOR/MONITOR'S REPORT NUMBER(S)

12. DISTRIBUTION / AVAILABILITY STATEMENT
Public Availability.

13. SUPPLEMENTARY NOTES

14. ABSTRACT

The research reported include the transitioning of previous work developed with semiconductor materials to new magnetic materials that may potentially lead to the development of magnetic storage devices with higher storage capabilities and other such devices. We have successfully grown and optimized the process of synthesizing single crystal annealed wires of ZnS materials as well as CoPt wires grown on an engineered viral template. The first known synthesis of $SmCO_5$ nanoparticles was achieved and conditions were further optimized for the synthesis and characterization of such materials. Additionally, viral screening of $SmCO_5$, FePt and CoPt was performed and the identification of specific binding peptides was achieved. Growth of these magnetic materials on both specific viral-bound and synthetic peptides was extended and further optimized. Ferromagnetic properties of such materials grown via viral templates are just now being explored, as are changes in synthetic conditions for optimal growth. Finally, further genetic engineering of the viral templates is underway, with successful formation of viral ring structures. These structures will continue to be altered and engineered for the directed synthesis of magnetic and electronic materials, potentially evolving into the next generation of memory cells, magnetic films and self-assembling rings and tubes that act as giant dipoles.

15. SUBJECT TERMS
Phage, Viruses, Self-assembly, Magnetic Nanowires

16. SECURITY CLASSIFICATION OF:			17. LIMITATION OF ABSTRACT	18. NUMBER OF PAGES	19a. NAME OF RESPONSIBLE PERSON
a. REPORT	b. ABSTRACT	c. THIS PAGE	UL	13	Angela M. Belcher
Unclassified	Unclassified	Unclassified			19b. TELEPHONE NUMBER *(include area code)* 617-324-2800

Air Force Performance Report

September 2003

PI: Angela Belcher

Massachusetts Institute of Technology
77 Massachusetts Ave, 16-244
Cambridge, MA 02139

Agreement Number: F49620-03-1-0319

Objectives:

Status of effort: The research funded through this grant focuses on a parallel approach to nanostructure self-assembly, using evolutionarily-selected, engineered peptides. This approach utilizing viral display and viral-based templates provides specific biological-inorganic interactions for materials assembly with a one "pot" synthesis, resulting in a simultaneous self-assembly process of bio-inorganic superstructures. Without biological-inorganic specificity, a *serial* processing strategy must be followed, in which each of the different types of nanocrystals are grafted to the biological molecules in isolated pots before mixing. Essentially, a truly biomimetic process, in which *all* of the building blocks are contained in the same reaction environment and self-assemble in a very specific manner can be realized by developing biomolecules with biological-inorganic specificity.

The research accomplished to date under the funding of this grant has strengthened the foundation of such an approach to materials design that has been explored by our lab for electronic and magnetic materials self-assembly. The specifics of experiments performed are detailed in the next section, and include the transitioning of previous work developed with semiconductor materials to magnetic materials that may potentially lead to the development of magnetic storage devices with higher storage capabilities and other such devices. We have successfully grown and optimized the process of synthesizing single crystal annealed wires of ZnS materials as well as CoPt wires grown on an engineered viral template. The first known synthesis of $SmCO_5$ nanoparticles was achieved and conditions were further optimized for the synthesis and characterization of such materials. Additionally, viral screening of $SmCO_5$, FePt and CoPt was performed and the identification of specific binding peptides was achieved. Growth of these magnetic materials on both specific viral-bound and synthetic peptides was extended and further optimized. Ferromagnetic properties of such materials grown via viral templates are just now being explored, as are changes in synthetic conditions for optimal growth. Finally, further genetic engineering of the viral templates is underway, with successful formation of viral ring structures. These structures will continue to be altered and engineered for the directed synthesis of magnetic and electronic materials, potentially evolving into the next generation of memory cells, magnetic films and self-assembling rings and tubes that act as giant dipoles.

Specific Accomplishments / New Findings:

I. Heated Wires

Our work funded under this grant has been taking the basis of earlier research discovered in our lab, namely the engineered pVIII viral wires, and further converting them through a heat transformation process into single crystalline nanowires. Evolution of substrate specific peptide scaffold was performed using phage display that has been previously reported by our group and serves as the basis for the material specificity in the viral based

template. Screening of the ZnS and CoPt systems using a disulphide constrained heptapeptide library yielded the consensus sequences CNNPMHQNC (termed A7) and ACNAGDHANC (termed CP7), respectively. The incorporation of these peptides into the highly ordered, self assembled capsid of the M13 Ff bacteriophage virus provided a linear template which simultaneously controlled particle phase and composition, with an added feature of material adaptability through genetic tuning of the basic protein building blocks.

Prior to annealing on silicon oxide TEM grids, nanocrystals (3~5 nm) grown on the virus surface for the ZnS system were in hexagonal wurtzite crystal structure, in close contact and preferentially oriented with both the [001] direction and the (100) plane perpendicular to the wire length direction which is supported by electron diffraction (ED), high resolution transmission electron microscopy (HRTEM), and dark-field transmission electron microscopy (TEM) diffraction-contrast imaging (Figure 1). The unannealed virus-CoPt system was of the $L1_0$ phase as evident by the characteristic (001) and (110) lines evident in the large area electron diffraction pattern and shows the polycrystalline nature of the material.

Annealing of the assemblies from 350-550°C promoted the growth of single crystal ZnS (Figure 1) and CoPt nanowires (Figure 2)of their respective phases that were uniform in diameter and on the length scale of the viral template (660nm). Annealing of the ZnS mineralized viruses allowed the polycrystalline assemblies to rapidly form single crystal wurtzite nanowires through removal of the template with a preferred orientation along both the [001] direction and (100) plane perpendicular to the wire length direction, as was seen prior to annealing. The single crystal nature of the CoPt wires was seen by selected area diffraction pattern, which also shows the characteristic $L1_0$ peaks, and by high resolution TEM lattice imaging showing the (111) plane perpendicular to the long axis of the wire. The persistence of the $L1_0$ phase, which is thermodynamically favored above 550° C, is attributed to the propensity of particles to maintain their orientation during aggregation based crystal growth. Although evidence of preferred crystallographic orientation among the unannealed CoPt particles is not as clearly identifiable as in the ZnS system, the single crystal nature of the nanowires implies that a large degree of order was present prior to annealing.

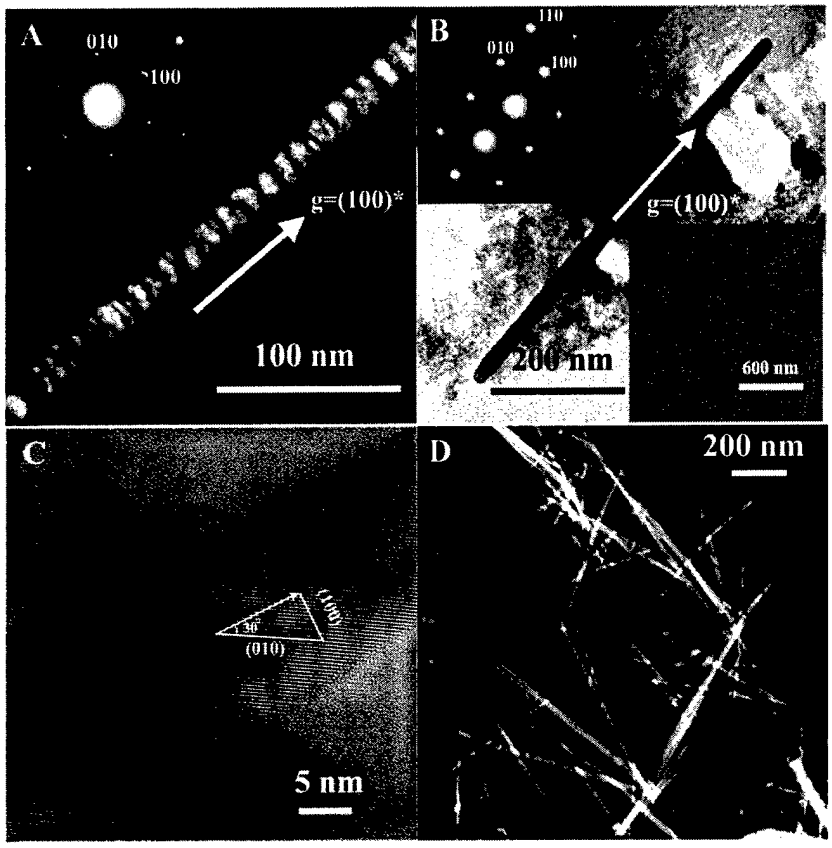

Figure 1. Advanced electron microscopy analysis of the precursor viral poly-nanocrystalline wires and the resultant single crystal ZnS nanowires after annealing. (A) Dark Field diffraction contrast imaging of the ZnS unannealed system using (100) reflection reveals the crystallographic ordering of the nucleated nanocrystals, where brighter contrast stems from the nanocrystals satisfying the (100) Bragg diffraction condition. Inset, ED pattern from a portion of the polycrystalline precursor wire flattened under TEM condition shows the hexagonal wurtzite crystal structure and the single crystal type [001] zone axis pattern. (B) Bright-field TEM image of the annealed ZnS single crystal nanowires. Inset (upper left), ED pattern of the individual nanowire, which was recorded along the [001] zone axis shows the single crystal of the wurtzite structure and suggests the single crystal nanowire inherits the preferred orientation of the precursor viral wire shown in (A). Inset (lower right), low magnification TEM image shows the monodispere isolated single crystal nanowires. (C) A typical HRTEM lattice image of a ZnS single crystal nanowire, which extends the length of the wire, showing the single crystal nature of the whole nanowire. The experimental lattice fringe spacing, 0.33 nm, is consistent with the 0.3309 nm separation between two (010) planes in bulk wurtzite ZnS crystals. The 30° orientation of (010) lattice planes with respect to the nanowire axis is consistent with the (100) growth direction determined by ED shown in (B). (D) HAADF STEM image of single crystal ZnS nanowires, which were annealed on a silicon wafer, and transferred from the silicon wafer to a TEM grid through ultrasonication in ethanol and centrifuge, shows the ability to produce multiple wires, with uniform diameters and lengths corresponding to single virus and aggregated virus particles.

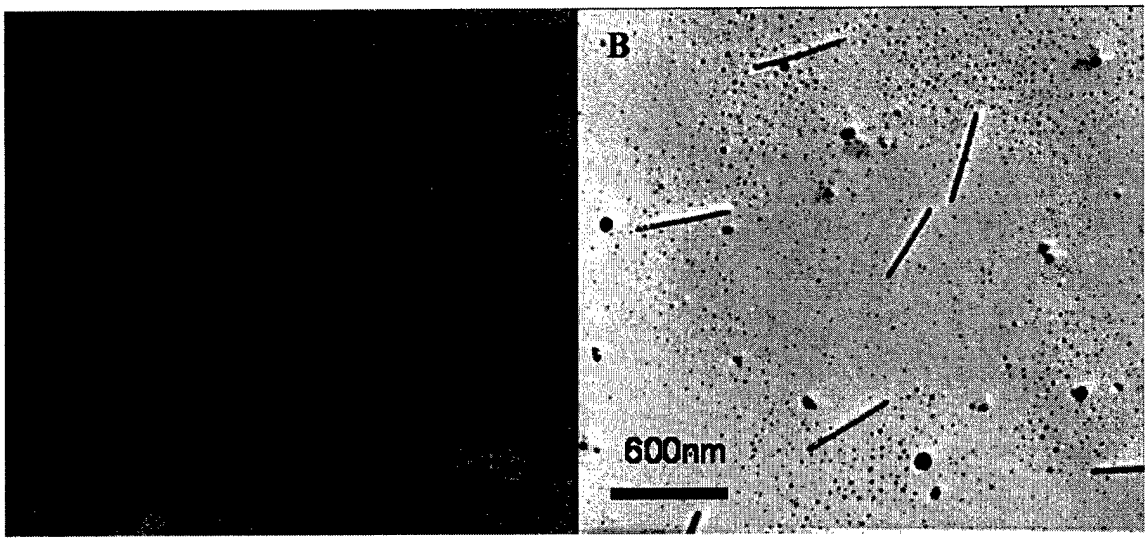

Figure 2: (A) Preannealed viral-based CoPt wires exhibit larger aggregation effects as compared to the ZnS system. (B) post annealing TEM images show the flexibility of the viral template yielding single crystal CoPt nanowires.

Computational analysis of peptide expression on the capsid of the virus revealed that the nearest neighbor peptide separation stabilized around 3nm at and above 20% peptide incorporation into the viral system; consequently high incorporation of the substrate specific fusion peptides is not required for complete mineralization of the virus to occur. Monte Carlo simulations of the A7 constrained sequence resulted in a 21% decrease in the standard deviation of backbone dihedral angles upon transfer of the peptide from isolation into the capsid environment, demonstrating the rigidity imposed on the fusion peptide. Ordering of the nucleated nanocrystals with regards to preferred crystallographic orientation along the length direction of the virus is believed to be a result of the stability of the peptide fusion and the symmetry of the virus coat.

II. Synthesis of nanoparticles composed of rare earth/transition metal alloys

Inorganic synthesis of rare earth/transition metal alloy nanoparticles. We have been working on the first reported synthesis of nanoparticles composed of rare earth/transition metal alloys. In the bulk, these materials display some of the highest recorded magnetic coercivities, up to 400 kOe for $SmCo_5$, making them excellent candidates for future magnetic storage devices with denser storage capability.

An arrested precipitation approach was taken to prepare nanoparticles of $SmCo_5$. This technique was adapted from previous efforts used to prepare Co nanoparticles. Transmission electron microscope (TEM) images of the as-prepared $SmCo_5$ nanoparticles reveal nanoparticles with an average diameter of 3.1 ± 0.7 nm. The corresponding selected-area electron diffraction pattern shows a ring pattern representing planes from

the hexagonal close packed (HCP P6/mmm) $SmCo_5$ crystal structure, including the (101), (201), and (301) planes. Since the diffraction pattern matches a hexagonal $SmCo_5$, it strongly suggests the formation of nanoparticles composed of the desired hexagonal $SmCo_5$ and not the most common rhombohedral phase.

The $SmCo_5$ nanoparticles were then annealed at 550 °C for 30 minutes under 5% H_2. The particles became much larger and very polydisperse, ranging from 5 nm to 25 nm in diameter. High resolution TEM images of the annealed $SmCo_5$ nanoparticle revealed distinct lattice planes with a spacing of 0.246 nm, corresponding to the (110) facet of HCP P6/mmm $SmCo_5$. Scanning Transmission Electron Microsopy (STEM) images indicated that the nanoparticles possessed a great deal of topography, again suggesting aggregation of smaller particles during the annealing process.

To reduce the oxidation of the $SmCo_3$ nanoparticles, a Pt deposition, based on the polyol process, was applied as a coating. TEM characterization of these nanoparticles, including high resolution TEM of the as-prepared nanoparticles (Figure 3A), selected area electron diffraction (Figure 3B), low resolution TEM of the annealed particles (3C), and selected area diffraction of the annealed particles (3D) showed spheres with an average diameter of 2.7 ± 0.5 nm. This was slightly smaller than the original particles because the Pt-coating was performed after a size-selective precipitation. HRTEM showed several facets, suggesting the as-prepared nanoparticles were single crystals, with facets typically have a spacing of 0.21 nm, corresponding to the (111) plane of Pt. Figure 3C shows that the coated nanoparticles behave in a similar fashion to the non-coated samples upon annealing, with extensive particle aggregation and polydispersity.

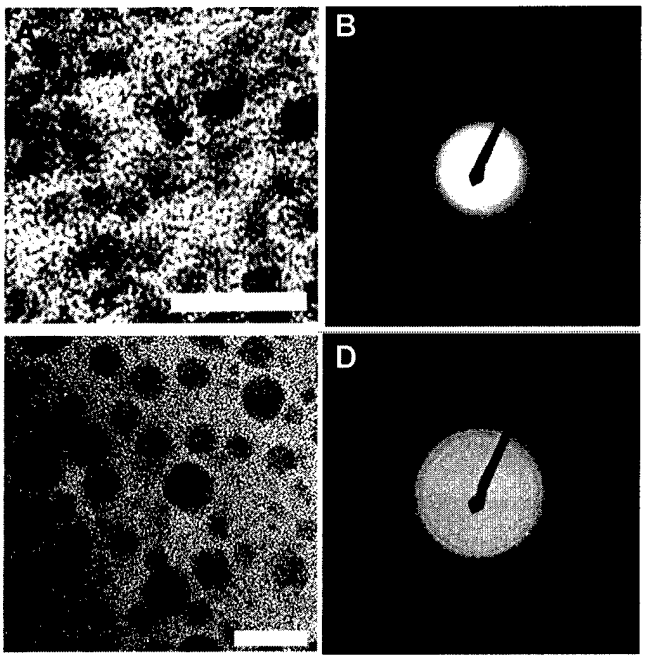

Figure 3: TEM characterization of Pt-coated $SmCo_5$ nanoparticles, including high resolution and selected area electron diffraction of the as-prepared particles and low resolution and selected area electron diffraction of particles annealed at 550°C for thirty minutes. Scale bars are 10 nm in A and C.

To determine if the particles had ferromagnetic proprties, the annealed $SmCo_5$ nanoparticles were characterized using a DMS Model 10 vector VSM. The resultant hysterisis loop of the annealed $SmCo_5$ nanoparticles taken at 150 K showed that the particles possessed a coercivity of 492 Oe, indicating that they were ferromagnetic. Changes in magnetic properties are currently being evaluated over a range of temperatures, from 150 K to 350 K. A hysteresis loop measured on Pt-Coated annealed $SmCo_5$ nanoparticles was also done. The coercivity of these particles was seen to be much higher than the noncoated samples at room temperature. This increase in coercivity is most likely a result of the decrease in oxidation and preservation of the magnetic HCP $SmCo_5$ phase. Additional experiments are under way to further characterize the magnetic properties of the Pt-coated $SmCo_5$ nanoparticles. It is important to note that the as-prepared nanoparticles are superparamagnetic at room temperature.

Bio-Inorganic synthesis of rare earth/transition metal alloy nanoparticles.
The biological synthetic strategy using M13 bacteriophage screening to subsequently grow nanoparticles with the identified material-specific peptides was applied to the $SmCo_5$ nanoparticles as well as other related technologically important magnetic materials, including FePt and CoPt. The magnetic materials screened were the $L1_0$ phases of FePt and CoPt as well as the annealed $SmCo_5$ materials synthesized above. After five rounds of screening, dominant sequences emerged from the phage display process. For FePt the dominant sequence was HNKHLPSTQPLA. The CoPt screening process yielded a peptide with the sequence KTHEIHSPLLHK. The $SmCo_5$ screening yielded the sequence WDPYSHLLQHPQ. The peptides selected in these experiments, which bind specifically to magnetic materials, may be able to exhibit similar control over the crystallization of magnetic nanostructures. The peptides isolated for the magnetic materials were used in this way, analogous to previous methods used by our lab.

Transmission electron microscopy (TEM) was used to observe nanoparticles prepared using the material-specific viruses isolated from the library (Figure 4). The images shown have been extensively characterized and conditions optimized. The FePt nanoparticles had an average diameter of 4.0 ± 0.6 nm, with lattice spacings of 0.22 nm, in good agreement with the literature values of $L1_0$ FePt. Additionally, the selected area electron diffraction pattern indicated these nanoparticles were composed of $L1_0$ FePt, with rings corresponding to the (110), (111), (201), (220) and (222) facets. The CoPt nanoparticles had an average diameter of 3.5 ± 0.7 nm. High resolution TEM images of CoPt nanoparticles prepared similarly to the FePt sample showed lattice spacings of 0.27 nm, similar to literature values of 0.269 nm for the (110) facet of CoPt. The selected area electron diffraction pattern of these nanoparticles also indicated the presence of the $L1_0$ phase of CoPt, and the reflection rings were assigned to the same facets as the $L1_0$ FePt. Only noncrystalline and polycrystalline nanoparticles were found in control experiments

involving phage that express a random peptide, wild-type phage that do not express any insert, and no phage.

Further, the FePt and CoPt-specific sequences were expressed as inserts on the pVIII protein of the bacteriophage using a technique previously described by our lab, and used as templates to grow nanocrystals. The data has been extensively analyzed and conditions optimized since the preliminary data was reported just 5 months ago. For x-ray analysis, the particles were slightly modified by adding 3-mercaptopropylsulfonic acid to the as-prepared particles and washing them with extensive amounts of acetonitrile in an attempt to remove the organics resulting from the viral propogation. The presence of the (110) peak in the diffraction pattern suggested the formation of the $L1_0$ phase of FePt. The peaks at 35 and 39 2-theta correlated to the residual NaCl and iron oxide respectively. From analysis of the CoPt samples by TEM, HRTEM, STEM and HAADF STEM, it was apparent that both Co and Pt are being nucleated along the entire coat of the phage, suggesting that the nanoparticles are composed of an alloy of Co and Pt (Figure 5).

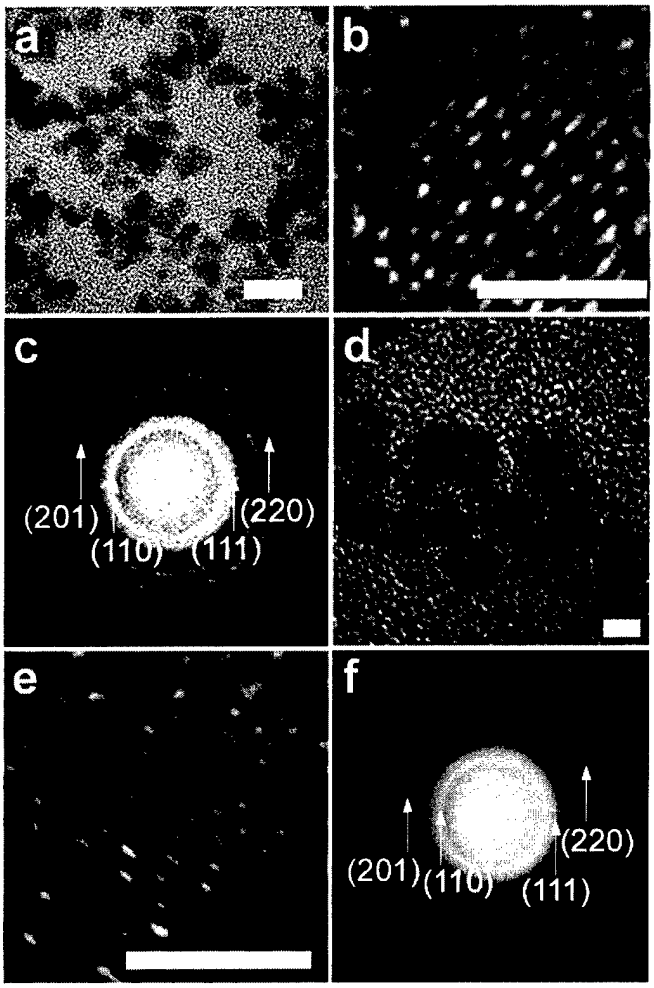

Figure 4: TEM characterization of as-prepared nanoparticles, including low resolution (a), high resolution (b) , and selected area electron diffraction (c) for FePt nanoparticles grown using bacteriophage that express the FePt-specific dodecapeptide. Low resolution (d), high resolution (e), and selected area electron diffraction (f) for CoPt nanoparticles grown using bacteriaphage that express the CoPt-specific dodecapeptide to template nanoparticle growth. Scale bars are 10 nm in a and 2 nm in c, d, and e.

Hysteresis loops for these particles at 5 and 300 K showed coercivities of 200 and 1350 Oe for FePt and CoPt, respectively (Figure 5). The presence of ferromagnetic material at room temperature indicates that $L1_0$ CoPt was being formed. A coercivity of 200 Oe was much lower than values reported for FePt nanoparticles, but literature nanoparticles typically are annealed, causing extensive cross-linking and aggregation. This aggregation leads to larger particle size, which will cause higher coercivity. M_s and m_r values for our particles particles were 2.2×10^3 and 2.0×10^{-4} emu, respectively, leading to a remanence ratio of 0.09. This low remanence ratio indicated that the particles are well-dispersed, and the only interparticle interactions were dipolar in nature. A similar set of hysteresis loops for FePt nanoparticles prepared using p8 expression were seen, with similar coercivity values and trends in saturation virtually identical to the CoPt nanoparticles.

To further investigate the effect of peptide concentration on nanoparticle nucleation, the FePt-specific dodecapeptide was prepared synthetically and used in particle nucleation experiments. The nanoparticles grown in the presence of the synthetic peptide had an average diameter of 4.1 ± 0.6 nm, and high resolution TEM imaging showed the presence of lattice fringes, with a spacing of 0.22 nm. X-ray diffraction data indicated that these nanoparticles were truly composed of $L1_0$ FePt. SQUID characterization at 300K indicated that these nanoparticles were ferromagnetic at room temperature, possessing a coercivity of 670 Oe. This value of coercivity is much higher than the coercivity found for as-prepared FePt nanoparticles synthesized using a more traditional solution chemistry approach, which only become ferromagnetic at room temperature after annealing.

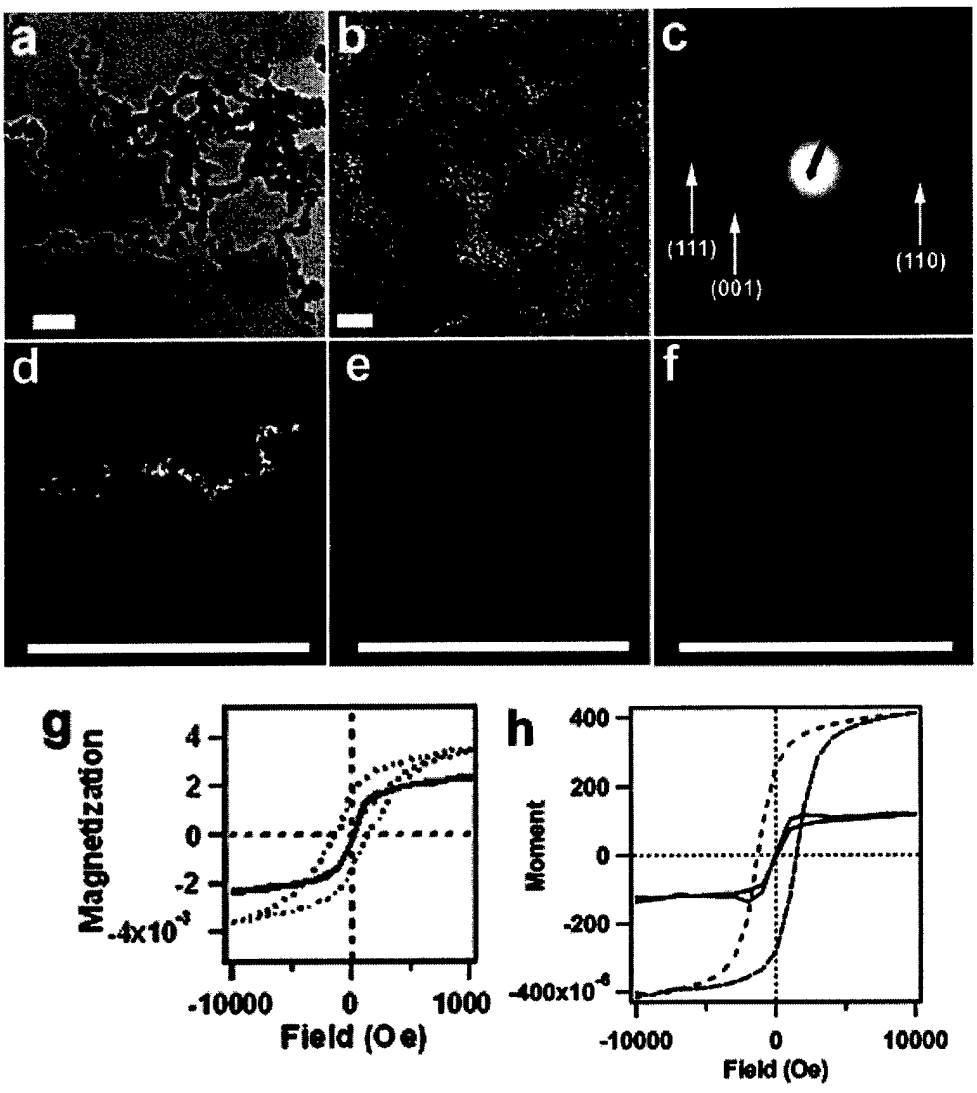

Figure 5: Characterization of CoPt nanoparticles grown on viruses that are genetically engineered to express the CoPt-specific peptide on their p8 coat protein including low resolution TEM (a), high resolution TEM (b), electron diffraction (c), STEM mapping (d), Pt mapping (e), Co mapping (f), and SQUID characterization of identical particles taken at 5 K (dotted line) and 300 K (solid line) (g). SQUID data for FePt nanoparticles grown on viruses engineered to express the FePt-specific peptide is also included (h), including hysteresis loops taken at 5 K (dotted line) and 300 K (dashed line). Scale bars in a and b are 50 nm and 2 nm respectively. Scale bars in d-f are all 700 nm.

The ferromagnetic materials synthesized in these experiments are radically different from ionic solids prepared using precipitation reactions. These materials are metallic alloys and are prepared by the reduction of metallic ions. The application of this technology to radically different materials and different chemical reactions suggests that peptides have the potential to fabricate a variety of inorganic materials that are not naturally evolved to coexist with biological systems. However, this control over organization and length scale that biology has fine tuned can be applied to these technologically important materials. This approach to synthesizing inorganic materials is more environmentally friendly

because it does not require halogenated organic solvents like the alternative preparations. Additionally, the protocol is very robust and could be applied to alternative magnetic materials.

III. Viral pIX engineering

Our previous work has shown that biomolecules, such as genetically engineered M13 bacteriophage (or viruses), can be used as molecular building blocks to nucleate and arrange quantum dots, to template semiconductor nanowires, and to build multidimensional liquid crystals and films. We are now further engineering viruses to demonstrate the one-dimensional (1D) formation of a ring structure and potentially of other interesting structures.

This virus-based ring structure is expected to function as a biological template for the nucleation and formation of metalized, magnetic, or semiconductor nanorings using a trifunctionalized virus. Modification of the pVIII with peptides that nucleate ZnS, CdS, or FePt nanowires has already been demonstrated. Magnetic ring structures have unique magnetic properties and are of interest for use as a magnetic data storage device. In addition, ring formation was designed to be reversible through regulation of of His_6 – NiNTA binding via control over free imidazole concentration. This and other reversible biomolecular interactions may enable engineered virus to function as a biomolecule based switch, which is similar in concept to a supramolecular switch.

Ring structures of M13 viruses were constructed by two genetic modifications of the M13 virus and synthesis of a heterobifunctional linker molecule, which was designed to bind each modified virus end. An anti-streptavidin peptide (Ser-Trp-Asp-Pro-Tyr-Ser-His-Leu-Leu-Gln-His-Pro-Gln) identified through a phage library screen for streptavidin binding, was displayed on one end of the virus. At the other end of the virus was fused a hexahistidine peptide, which binds strongly to Ni(II)-nitrilotriacetic acid complex (Ni-NTA). A linker molecule consisting of streptavidin conjugated with Ni-NTA was also synthesized. Addition of a linker molecule triggered the ring formation reaction, which was therefore preprogrammed and inducible.

Various concentrations of the bifunctional virus and linker molecule were mixed and the structures imaged by AFM (Figure 6a). The viruses were observed to form a ring structure when the inter distance of each M13 virus in solution was greater than a few times the virus length, and the relative concentration of the M13 virus to NiNTA-streptavidin was 1:1. The ring formation verified the successful engineering of the both ends of the virus to generate a bifunctional M13 virus. The radii of the rings were in the range of 70 nm to 100 nm. The circumference corresponded to the size of the filamentous virus produced from the viral system. This to our knowledge is the first engineered bifunctional M13 virus.

The size of the observed ring by TEM was similar to that of the ring structure in AFM image. Antibody labeling was used to enhance the contrast of the virus rings for TEM imaging. A polyclonal pVIII primary antibody was used to bind the major coat of the virus and anti-rabbit IgG secondary antibody conjugated to10 nm gold nanoparticle was used as the label, as shown in Figure 6b. The large effective diameter of the antibody conjugated gold particles potentially distorts the size of the observed virus rings. However, ring shaped assembly of gold nanoparticles were observed in the sample.

When the concentration of the virus was high enough for multiple viruses to collide with a linker, they linkED together linearly or radially. Virus and linker were mixed at a ratio of 10:1 (10^{12} units/mL:10^{11} units/mL) and observed by AFM, as shown in figure 5. As a result, by simply controlling the concentration of the virus and the linker in this system, various self-assembling structures were achieved.

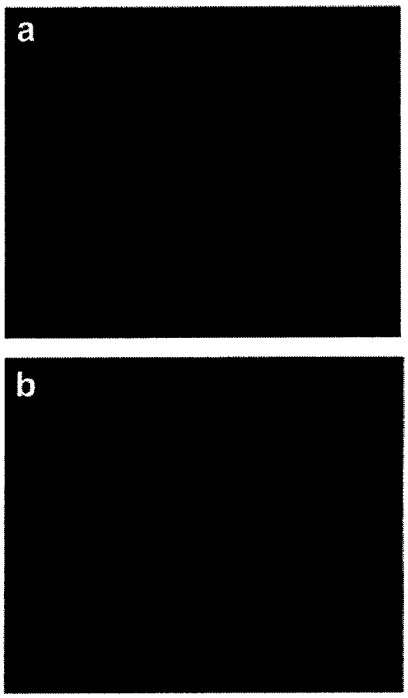

Figure 6: a, AFM images of the viral ring structures; b, TEM images of the ring formation tagged with a polyclonal pVIII primary antibody conjugated to gold nanoparticles.

Personnel Supported:

Angela Belcher, PI (1 month summer salary)
Jifa Qi, Postdoctoral Associate (25%)
Brian Reiss, Postdoctoral Associate (0%, Full Fellowship)
Sreekar Bhaviripudi, Graduate Student (100%)
Steven Kottmann, Graduate Student (100%)
Ki Tae Nam, Graduate Student (0%, Full Fellowship)
Beau Peelle, Graduate Student (0%, Full Fellowship)

Publications:

Chuanbin Mao, Daniel J. Solis, Stephen T. Kottmann, Rozamond Y. Sweeny, Brian D. Reiss, and Angela M. Belcher. "Virus Based Scaffolds for the Peptide Directed Synthesis of Single Crystal Magnetic and Semiconducting Nanowires." Submitting to *Science*, 2003.

Brian D. Reiss, Chuanbin Mao, Thomas Thomson, and Angela M. Belcher. "Synthesis of $SmCo_5$ and Pt-Coated $SmCo_5$ Nanoparticles." Submitting to *Advanced Materials*, 2003.

Brian D. Reiss, Chuanbin Mao, Daniel J. Solis, Rozamond Y. Sweeney, Katherine S. Ryan, Anuj Aggarwal, Thomas Thomson, and Angela M. Belcher. "Biological Routes to Metal Alloy Ferromagnetic Nanostructures." In review, *Nature Materials*, 2003.

Ki Tae Nam, Beau R. Peelle, Seung-Wuk Lee and Angela M. Belcher. "Genetically driven assembly of nanorings based on the M13 virus." Submitting to *NanoLetters*, 2003.

Consultive/Advisory Functions:

Defense Science Study Group
JASON
NRC Solid State Physics Board
Editorial Committee Annual Reviews of Materials Research
Editorial Committee Board of Nanotechnology
Editorial Committee Advanced Functional Materials

New Discoveries, Inventions or Patent Disclosures:

None